Journal of Orthopaedic Translation 38 (2023) 23–31

Contents lists available at ScienceDirect

Journal of Orthopaedic Translation

journal homepage: www.journals.elsevier.com/journal-of-orthopaedic-translation

original article

Peptide modified geniposidic acid targets bone and effectively promotes osteogenesis

Meijing Liu [a,b,1], Danqi Zhu [a,1], Fujun Jin [a,1], Shuang Li [a], Xiangning Liu [b], Xiaogang Wang [a,*]

[a] Key Laboratory of Big Data-Based Precision Medicine, School of Engineering Medicine, Beihang University, Beijing, 100191, China
[b] Clinical Research Platform for Interdiscipline of Stomatology, The First Affiliated Hospital of Jinan University & Department of Stomatology, Jinan University, Guangzhou, 510632, PR China

ARTICLE INFO

Keywords:
Geniposidic acid
SDSSD
Bone targeting
Osteogenesis

ABSTRACTS

Background: Geniposidic acid (GPA), one of the active components of Eucommia ulmoides, promote bone formation and treat osteoporosis by activating farnesoid X receptor (FXR). However, GPA has low oral availability and lack of bone targeting in the treatment of bone related diseases. With the development of modern technology, small molecules, amino acids, or aptamers are used for biological modification of drugs and target cells in bone tissue, which has become the trend of bone targeted research.

Methods: In this study, SDSSD (an osteoblast-targeting peptide) were modified in GPA using Fmoc solid-phase synthesis technique to form a new SDSSD-GPA conjugate (SGPA). The bone targeting of SGPA was evaluated using in vivo imaging and cell co-culture. In vitro, the effect of SGPA on cytotoxicity, osteoblastic activity, and mineralization ability were studied in mouse primary osteoblasts (OBs). *In vivo*, the therapeutic effect of SGPA on osteoporosis using an ovariectomized (OVX) mouse model. The bone mass, histomorphometry, serum biochemical parameters, and the molecular mechanism were evaluated.

Results: SGPA was enriched in OBs and tends to accumulate in bone tissue. In vitro, SGPA significantly enhanced the osteogenic activity and mineralization of OBs compared with GPA. In vivo, SGPA enhanced serum BALP and P1NP levels, increased the trabecular bone mass of the mice, and SGPA administration have a higher bone mineralization deposition rate than the GPA-treated mice. Moreover, SGPA significantly activated FXR and Runt-related transcription factor 2 (RUNX2).

Conclusions: Collectively, SGPA is enriched into OBs, and promotes bone formation by activating FXR-RUNX2 signalling, effectively treating osteoporosis at relatively low doses.

The translational potential of this article: This study demonstrates a more efficient and safe application of GPA in treating osteoporosis, provide a new concept for the bone targeted application of natural compounds.

1. Introduction

Bone is undergoing bone reconstitution, and the imbalance of this process will lead to a variety of metabolic disorders, such as osteoporosis, Paget's disease, hypercalcemia, osteoarthritis. Among them, approximately 200 million people worldwide suffer from osteoporosis [1], and approximately 12.3 million American [2] and 60.2 million Chinese [3] over age 50 suffer from primary osteoporosis. However, the clinical treatment of osteoporosis drugs is limited and associated with significant complications [4,5]. Therefore, osteoporosis has become one of the three major geriatric diseases that are mainly solved globally.

Geniposidic acid (GPA) is an iridoid glucoside and one of the active components of Eucommiae cortex extract, which has promoted osteogenesis [6,7] and hepatoprotective activity [8]. Like existing anti-osteoporosis drugs, GPA is not target the bone, but enriched in liver and kidney [9,10]. Moreover, as a bile acid receptor, farnesoid X receptor

Abbreviations: ALP, alkaline phosphatase; BALP, bone alkaline phosphatase; BMD, bone mineral density; BMSCs, bone marrow mesenchymal stem cells; BSEP, bile salt export pump; BV/TV, relative bone volume; Ct.Th., cortical thickness; FXR, farnesoid X receptor; GPA, geniposidic acid; MAR, mineral apposition rate; OBs, osteoblasts; OCN, osteocalcin; OSF-2, osteoblast-specific factor 2; OVX, ovariectomized; P1NP, procollagen type I N-terminal propeptide; Runx2, Runt-related transcription factor 2; SDSSD, Ser-Asp-Ser-Ser-Asp; SGPA, SDSSD-GPA conjugate; Tb.N., trabecular number.

* Corresponding author. Key Laboratory of Big Data-Based Precision Medicine, School of Engineering Medicine, Beihang University, Beijing, 100191, China.
E-mail address: xiaogangwang@buaa.edu.cn (X. Wang).

[1] These authors contributed equally to this work

https://doi.org/10.1016/j.jot.2022.07.007
Received 10 May 2022; Received in revised form 29 June 2022; Accepted 15 July 2022

(FXR) is activated by GPA and is highly expressed in liver, intestine and bone [11,12]. In addition, the high hardness, poor permeability, low blood flow and physiological specificity of bone tissue make it difficult for drugs to reach bone tissue effectively [13]. Addressing the low bioavailability and lack of bone targeting of oral GPA could further broaden the clinical application of GPA or other natural compounds for the treatment of bone-related diseases.

The most important clinical goal in the treating bone related diseases is to achieve precise therapeutic efficacy in defined pathological sites. By endowing osteopathic agents with osteophilicity, their pharmacodynamic profile can be significantly altered to favourable bone deposition, and this bone tissue therapy regimen can effectively improve the local therapeutic index on a sustained basis [14]. Since the concept of bone-targeting was put forward, early studies mainly used drugs such as tetracycline and bisphosphonate [15,16], which have a specific affinity with hydroxyapatite, and specifically act on the whole bone tissue to improve the utilization rate of drug. With the development of biotechnology, the research of drug targeted specific cells of bone tissue is carried out, through the biological modification of drugs by special small molecules, amino acids, or aptamers [17,18]. For example, bone marrow mesenchymal stem cells (BMSCs) -specific aptamer [19,20] and osteoblast-specific aptamer CH6 [18] targeting BMSCs or osteoblasts (OBs) for the treatment of bone-related diseases. Previously, Ser-Asp-Ser-Ser-Asp (SDSSD), a small molecule peptide screened by phage technology, can specifically target both human and mouse OBs [21]. SDSSD has a high affinity with osteoblast-specific factor 2 (OSF-2) and has the functional advantage of targeting OBs. In addition, preferential accumulation of drugs in bone reduces systemic distribution to other tissues, significantly reducing systemic toxicity and long-term concern [22]. Compared with traditional therapy, local application of bone targeted therapy requires a smaller dose of therapeutic agent [22]. In view of these unique advantages, bone targeted therapy can serve as a promising therapeutic approach in the field of bone diseases.

In this study, GPA is modified by osteoblast targeted peptide SDSSD to form a new coupling molecule SGPA, effectively accumulate in OBs and play a role in promoting bone formation at low doses, providing a new perspective for the tissue- or cellular targeting of natural compounds with similar GPA structures.

2. Materials and methods

2.1. Materials

Geniposidic acid (GPA, $C_{16}H_{22}O_{10}$, molecular weight (Mw) = 374.34, 98.47% purity) was purchased from Linchuan Zhixin Biological Technology Co. LTD. (Jiangxi, China).

SDSSD peptides was purchased from Shanghai Qiangyao Biological Technology Co., LTD. (Shanghai, China).

2.2. Synthesis of SGPA and FAM-SGPA

The SDSSD-GPA (SGPA) was synthesized using standard Fmoc chemistry. Dry the SGPA product under vacuum, purify the SGPA by prep-HPLC (A: 0.075% TFA in H2O, B: ACN). The fluorescein amine (FAM) labelled SGPA (FAM-SGPA) was also synthesized using standard Fmoc chemistry. All products were characterized by LC-MS and H NMR, and purity was analyzed by HPLC. The synthesis of SGPA conjugate and FAM-SGPA were completed by WuXi App Tec (Shanghai, China).

2.3. Animal and experimental design

The use of laboratory animals was approved by the Institutional Animal Care and Use Committee of Beihang University (NO: BM20200046). C57BL/6J mice and Kunming mice were purchased from the Department of Laboratory Animal Science, Peking University Health Science Center (SCXK (Jing) 2016–0010, Beijing, China). Twelve-week-old female C57BL/6J mice were performed with ovariotomy (OVX) or sham operation. They were housed in specific pathogen free animal facility and were served standard laboratory chow and water. Three months after surgery, these mice were randomly divided into four groups with 6 animals/group, including Sham, OVX, OVX+20 mg/kg GPA, OVX+20 mg/kg SGPA. Dose administration was performed intravenously daily for 4 weeks. For sampling, the mice were anesthetized by intraperitoneal injection of sodium pentobarbital, the blood was collected. After the mice were sacrificed, the right femur was collected for micro-CT and histopathology analysis, and the left femur was harvested for mRNA and protein expression analysis.

2.4. Distribution of SGPA in vivo

Twelve-week-old female Kunming mice were anesthetized by intraperitoneal injection of sodium pentobarbital, then anesthetized mice were injected with FAM-SGPA (20 mg/kg). Mice were placed in IVIS Spectrum CT In Vivo Imaging System (PerkinElmer) for real-time fluorescence monitoring in vivo. In addition, mice were sacrificed at different times (2 h, 6h, 24 h, and 48 h), the brain, lung, heart, liver, spleen, kidney, and bone were isolated, and their fluorescence was observed by in IVIS Spectrum Imaging System.

2.5. Analysis of serum biomarker for bone formation

Blood was centrifuged at 1000 g for 10 min at 4 °C. The levels of serum bone formation biomarkers including bone alkaline phosphatase (BALP, #CSB-E11914m), procollagen type I N-terminal propeptide (P1NP, #CSB-E12775m) were measured using ELISA kit (Cusabio, Wuhan, China) following the manufacturer's instructions.

2.6. Micro-CT analysis

The right femurs of mice (n = 6) were scanned by micro-CT system (Bruker SkyScan 1276, Kontich, Belgium). The scanning resolution was set as 6 μm for one layer. The representative reconstruction image of femur was taken with the morphology of distal growth plate as reference. The bone mass analysis for trabecular bone was limited in 100 scanning layers upon distal femur growth plate, and 50 scanning layers of cortical bone was reconstructed for the statical analysis analysed. Base on three-dimensional (3D) images, we determined parameters such as bone volume fraction (BV/TV, %), trabecular number (Tb.N, 1/mm), cortical thickness (Ct.Th, mm), and mineral apposition rate (MAR, μm/d).

2.7. Fluorochrome double labelling analysis

The impact of SGPA on the bone formation rate analysis was performed as described previously [23]. In brief, xylenol orange (10 mg/kg) was injected into the mice via an intraperitoneal injection, after 2 weeks, calcein (20 mg/kg) was injected. Finally, the mice were killed, the femurs were collected and fixed in 4% PFA solution, embedded in light-cured resin, and were performed with a micro section and grinding system, cut into bone sections (4 μm thickness). The bone sections were rinsed and incubated with 4,6-diamidino-2-phenylindole (DAPI, Sigma) for 15 min followed by exhaustive washing in PBS. Images were obtained under a fluorescence microscope (Leica).

2.8. Cell culture

MC3T3-E1 cells were purchased from the cell bank of the Shanghai Institute (Shanghai, China). Mouse primary OBs were isolated from the neonatal C57BL/6 mice calvaria following the reference reported experimental procedures [24]. The cells were cultured at 37 °C in a humidified 5% CO_2 incubator with α-MEM (Gibco), 10% fetal bovine serum (FBS, Gibco), 1% antibiotic-antimycotic (100 U/mL penicillin and 0.1 mg/mL streptomycin, Gibco). Mouse osteoclasts (OCs) were

differentiated from mouse bone marrow cells (BMCs) with macrophage colony stimulating factor (M-CSF) and murine nuclear factor-κB ligand (RANKL) following previously reported experimental procedures [25].

2.9. Cell viability assay

Mouse primary OBs (4×10^3 cells/per well) were seeded in 96-well plates. 200 μL α-MEM containing SGPA (0, 1, 5, 10, 20, 50, 100, 200 μM) were added to each well after the cells adhered to the wells. Cell viability was tested after culturing for 48 h. The plates were rinsed with phosphate buffered saline (PBS, HyClone, USA) before the Cell Counting Kit-8 (CCK-8) assays (Dojindo, Japan). According to the manufacturer's instructions, 10 μL CCK-8 reagent and 90 μL α-MEM were added into each well, further incubated at 37 °C for 2 h. The OD of cells at 450 nm was measured by a microplate reader (Varioskan LUX, Thermo Fisher Scientific, MA, USA). Cell viability was calculated as (OD_{SGPA}-OD_{blk})/(OD_{ctrl}-OD_{blk}) × 100% (blk = blank, ctrl = control).

2.10. SGPA preference for osteoblasts, osteoclasts

Mouse BMCs were seeded in culture dish (#801001, NEST, China), adding osteoclasts differentiation media (α-MEM containing RANKL (50 ng/mL, #315–11, Pepro Tech, USA) and M-CSF (25 ng/mL, #315–02, Pepro Tech, USA)), replace OCs differentiation media every two days. After observing OCs fusing and forming multinucleated cells, then the OBs (AAV-CGA-mCherry-WPRE-SV40pA was transfected) were co-cultured for 24h. 1 mL α-MEM containing FAM-SGPA (10 μM) were added to culture dish, incubated for 24 h. Then the Hoechst 33,342 labelling solution (HY-15559A, MCE, New Jersey, NJ) were added and incubated for 15 min, aspirate the labelling solution. The cells were rinsed three times in PBS, added into the α-MEM, and observed under a confocal laser scanning microscope (Leica).

2.11. The cellular targeting ratio for SGPA in osteoblasts

Mouse primary OBs were seeded in culture dish (#801001, NEST, China). 1 mL α-MEM containing FAM-SGPA (10 μM) were added to culture dish after the cells adhered to the culture dish, incubated for 0.5 h, 1 h, 2 h, and 4 h. Then the Hoechst 3342 labelling solution were added and incubated for 15 min, aspirate the labelling solution. The cells were rinsed three times in PBS, added into the α-MEM, and observed under a confocal laser scanning microscope (Leica).

2.12. ALP activity analysis of MC3T3-E1 cells

MC3T3-E1 (2.5×10^5 cells/per well) were seeded in 6-well plates and cultured for 24 h, then cotreated with osteogenic differentiation medium (ODM) containing SGPA (2.5, 5, 10 μM) or GPA (50 μM) for 14 days, change the medium every two days. The levels of ALP activity were measured by commercial kit according to the manufacturer's protocols (BC2145, Solabio, Beijng, China). In short, the cells in extracting solution were broken by cellular ultrasonic crusher, centrifuged at 4 °C 10,000 rpm for 10 min, and the supernatant was taken for determination. The OD of supernatant at 510 nm was measured by a microplate reader (Varioskan LUX, Thermo Fisher Scientific, MA, USA). And, the levels of ALP activity were calculated according to the formula provided in manufacturer's instruction.

2.13. Alizarin red staining and mineralization

The MC3T3-E1 cells were cultured in ODM in the presence of different concentrations SGPA for 21 days, then the mineralization function of OBs was evaluated with alizarin red staining kit (Sigma–Aldrich). The staining procedures were performed according to the manufacturer's protocols. Representative histological images were obtained under an inverted microscope (Nikon, Tokyo, Japan).

2.14. RNA extraction and quantitative real-time PCR analysis

Total RNA was isolated from the bone tissues of mice, or MC3T3-E1 cells using RNAiso Plus (Takara, Tokyo, Japan). cDNA was synthesized using the PrimeScript™ RT Master Mix Kit (Takara, Tokyo, Japan), and real-time qPCR was performed using TB Green® Premix Ex Taq™ II (Takara, Tokyo, Japan) in an CFX96™ Real-Time System (Bio-Rad Laboratories, Hercules, CA) according to the manufacturer's protocol. The primer sequences used for amplification of *Bsep, Runx2* and glyceraldehyde-3-phosphate dehydrogenase (*Gapdh*) are listed below, *Bsep* (F: 5′-AGC AGG CTC AGC TGC ATG AC-3′, R: 5′-AAT GGC CCG AGC AAT AGC AA-3′), *Runx2* (F: 5′-GAC TGT GGT TAC CGT CAT GGC-3′, R: 5′-ACT TGG TTT TTC ATA ACA GCG GA-3′), *Gapdh* (F: 5′-TGT GTC CGT CGT GGA TCT GA-3′, R: 5′-TTG CTG TTG AAG TCG CAG GAG-3′). All experiments were performed in triplicates and analysed using the $2^{-\Delta\Delta Ct}$ method. For standardization and quantification, *Gapdh* mRNA was amplified simultaneously.

2.15. Western blotting analysis

Total proteins from MC3T3-E1 cells or bone tissues of mice were extracted with RIPA lysis buffer containing protease inhibitors (Sigma–Aldrich). The protein concentration was quantified by the bicinchoninic acid reagent kit (Beyotime, China). The proteins were separated by 10% SDS-PAGE and transferred to Immuno-Blot PVDF membranes (Merck Millipore, Germany). The membranes were then blocked with 5% BSA and overnight incubated with specific primary antibodies targeting BSEP (1:1000, Abcam, ab155421), RUNX2 (1:1000, Cell signalling Technology, 12,556), and GAPDH (1:3000, Abcam, ab8245) at 4 °C. The next day, the blots were then incubated in secondary antibody (horseradish peroxidase–labelled) for 1 h with shaking at room temperature, and the blots were visualized by SuperSignal chemiluminescent HRP substrates (Thermo Scientific) using Molecular Imager ChemiDOC™ XBS imaging systems (Bio-Rad Laboratories).

2.16. Immunofluorescence of bone tissues

The femur specimens were fixed in 4% PFA solution for 48 h. Specimens were rinsed in phosphate-buffered saline (PBS), and decalcification was performed in EDTA decalcifying solution (pH 7.2, #E1171, Solarbio, China) at room temperature for 1 month. EDTA decalcifying solution was replaced weekly. The specimens were washed in PBS and then embedded in paraffin, cut into bone sections (4-μm thick). Sections were dewaxed and rehydrated in ethanol at different concentration gradients. The slides were permeabilized with 0.2% Trition-X100 (Sigma–Aldrich), then blocked with 5% BSA for 1 h at RT in humidified chamber and incubated with primary antibodies FXR (Abcam, ab129089) and RUNX2 (Cell signalling Technology, 12,556) diluted in 5% BSA at 4 °C overnight. After washing in PBS, the sections were incubated with FITC- or Alexa 594-conjugated secondary antibodies at room temperature in the dark for 1 h. Nuclei were counterstained by incubation in 1 μg/mL 4',6-diamidino-2-phenylindole (DAPI; Solarbio, China) for 20 min followed by exhaustive washing in PBS. The sections were visualized with a fluorescence microscope (Leica).

2.17. Statistical analysis

All numerical data are expressed as the mean ± S.D. All statistical analyses were performed with SPSS software (v.16.0). One-way analysis of variance (ANOVA) followed by Bonferroni or Dunnett's T3 was performed for the statistical significance analysis of multiple comparisons. The Student's t-test was performed for the statistical significance analysis of the difference between two groups. The p values < 0.05 were considered statistically significant for all tests.

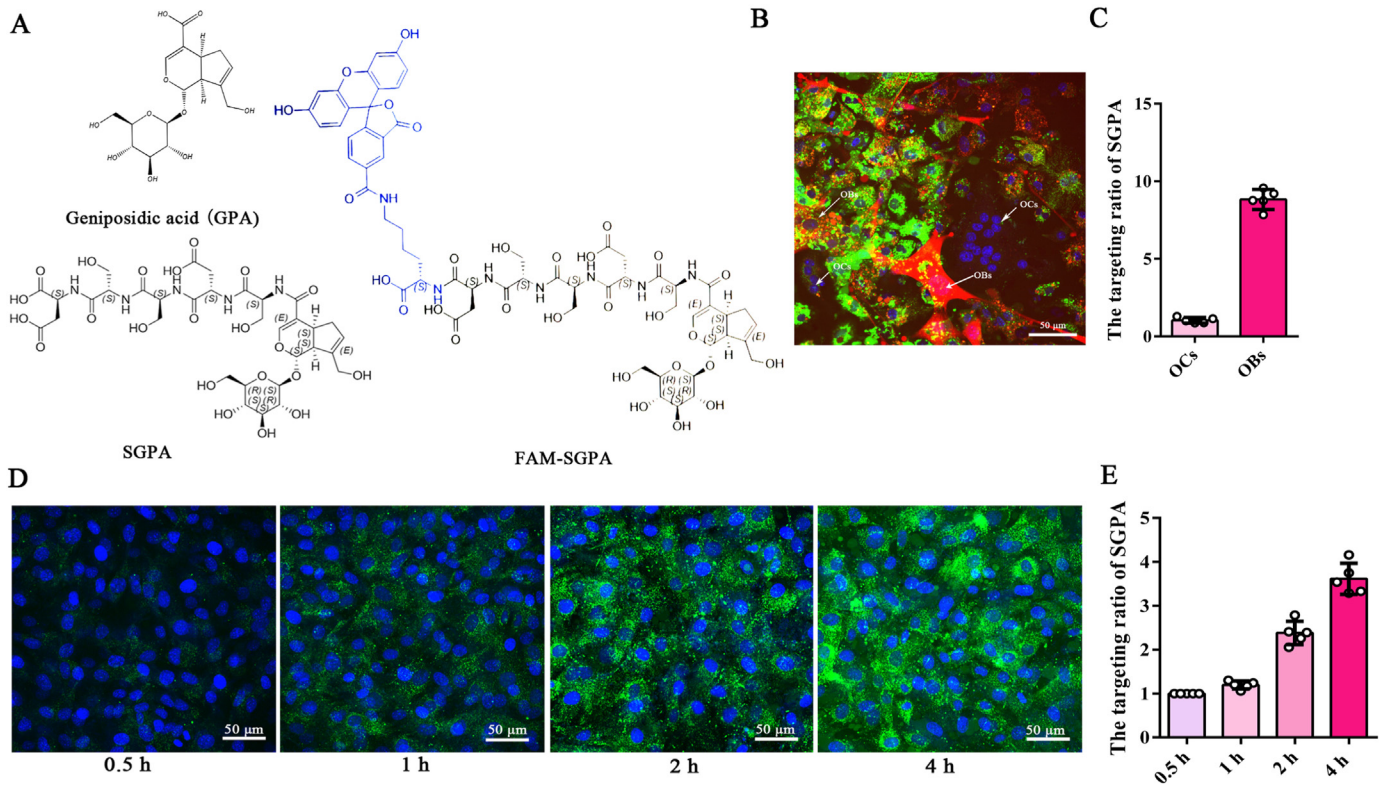

Figure 1. SGPA aggregates into osteoblasts in vitro. (A) The chemical structures of GPA, SGPA, FAM-SGPA. (B) OBs (red) and OCs were co-cultured, FAM-SGPA (green) were added to culture dish, incubated for 24 h, labelled the nucleus with Hoechst 33342 (blue), and observed under a confocal laser scanning microscope (magnification: 630 ×). (C) The cellular targeting ratio for SGPA in OBs and OCs. (D) FAM-SGPA (green) interfered with OBs for 0.5 h, 1 h, 2 h and 4 h, labelled the nucleus with Hoechst 33342 (blue), and observed under a confocal laser scanning microscope (magnification: 400 ×). (E) The cellular targeting ratio for SGPA in OBs at different times.

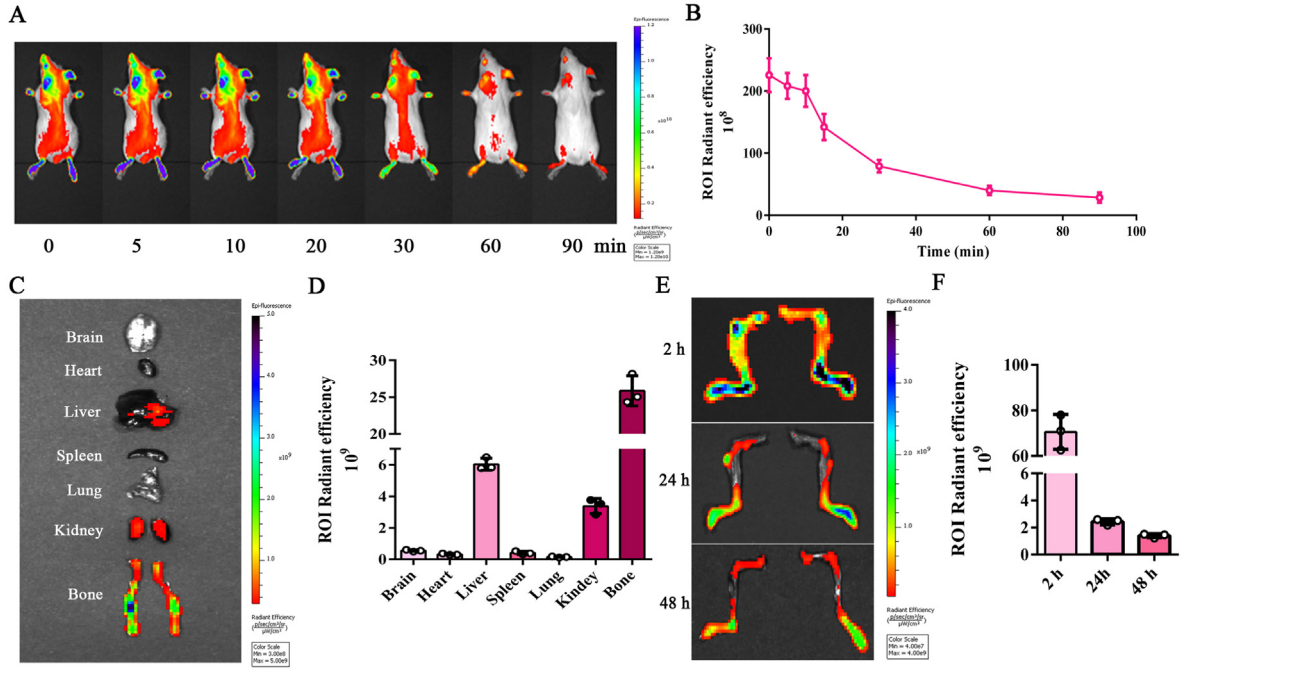

Figure 2. SGPA accumulates in bone tissue. (A) Anesthetized mice were injected with saline or FAM-SGPA via tail vein. Representative images of the biodistribution of SGPA in mice. (B) The radiant efficiency of FAM-SGPA in the hind limb was quantified. (C) Representative images of the biodistribution of FAM-SGPA in the brain, lung, heart, liver, spleen, kidney, and bone 6 h after being injected into the tail vein. (D) The radiant efficiency of FAM-SGPA in all tissues was quantified. (E) Representative images of the biodistribution of FAM-SGPA in bone tissues 2 h, 24 h, and 48 h after being injected into the tail vein. (F) The radiant efficiency of FAM-SGPA in bone tissues was quantified.

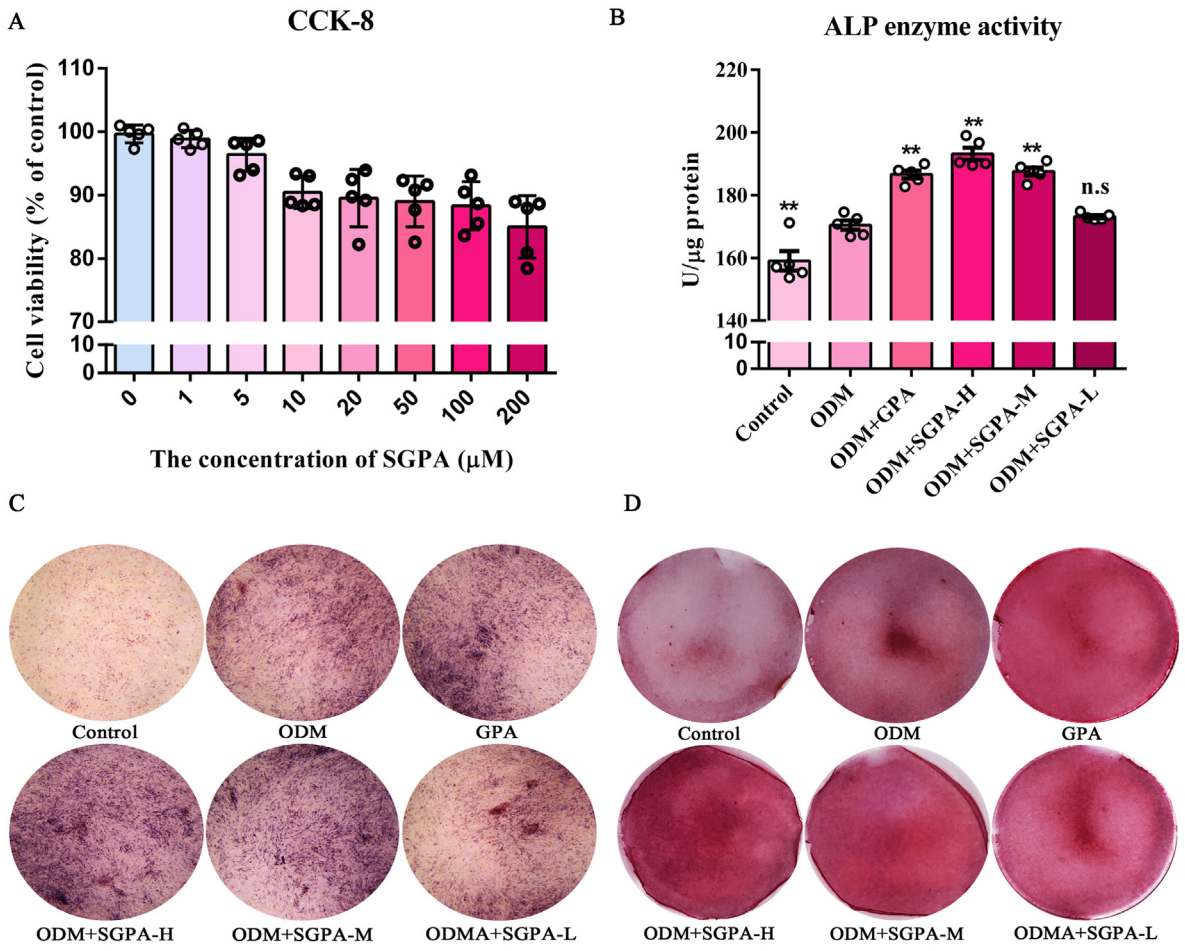

Figure 3. SGPA enhances osteoblast activity. (A) The effect of SGPA on cell viability was evaluated using CCK8 assay. (B) MC3T3-E1 cells were maintained for 7 days in osteogenic differentiation medium (ODM) with GPA (50 μM) or SGPA (2.5–10 μM), ALP enzyme activity was assessed. (C) MC3T3-E1 cells were maintained for 14 days in ODM with GPA (50 μM) or SGPA (2.5–10 μM). The cells were stained with ALP. (D) MC3T3-E1 cells were maintained for 21 days in ODM with GPA (50 μM) or SGPA (2.5–10 μM). The cells were stained with Alizarin Red. Data are presented as the means ± S.D. n.s not significant, $*P < 0.05$, $**P < 0.01$.

3. Results

3.1. SGPA aggregates into osteoblasts in vitro

To give the bone tissue targeting property of GPA, modified GPA with small molecule peptide SDSSD and synthesized a new SGPA conjugate. The structure and purity analysis are shown in Fig.S1. To explore the targeting of SGPA, we prepared a FAM probe for fluorescent labelling (Fig. 1A). And, the co-culture system of primary OBs and OCs was constructed, and the OBs were labelled with adeno-associated virus (AAV-CGA-mCherry-WPRE-SV40pA). FAM-SGPA was used to intervene the system for 24 h in vitro, and the uptake of SGPA in cells was observed. The results showed that SGPA was mainly taken up by OBs rather than OCs, confirming the specificity of SGPA targeting OBs (Fig. 1B).

The targeting of SGPA to OBs was further analysed, and FAM-SGPA was used to intervene primary OBs for 0.5h, 1h, 2h and 4h in vitro. The results showed that SGPA could be rapidly absorbed into the cytoplasm by primary mouse OBs, and part of SGPA reached the nucleus 4h later (Fig. 1C).

3.2. SGPA accumulates in bone tissue

In order to evaluate the distribution of SGPA in vivo, FAM-SGPA was injected into mice through the tail vein, and the distribution of SGPA in each tissue was monitored by IVIS spectrum imaging system. The results showed that SGPA was rapidly distributed in mice and bone tissue was significantly aggregated (Fig. 2A–B). The distribution of SGPA in brain, lung, heart, liver, spleen, kidney, and bone was evaluated. Imaging results showed rapid distribution of SGPA in bone, liver, and kidney, especially in bone tissue, which was 4 times as much as in liver (Fig. 2C–D). In addition, slight amount of SGPA could still be seen in bone tissue 24h and 48h (Fig. 2E–F). These results suggest that SGPA can rapidly distribute into bone tissue after entering the body.

3.3. SGPA enhances osteoblast activity in vitro

The effect of SGPA on cell activity was first evaluated. SGPA had a low toxicity to OBs at concentrations lower than 10 μmol/L (Fig. 3A). At this concentration range, the cell viability was approximately 90%. Therefore, SGPA at lower than 10 μmol/L was considered safe and the high, middle, and low concentration of SGPA are determined as 10, 5, 2.5 μmol/L, respectively. To determine the osteogenic activity of SGPA in mice, SGPA interfered with primary OBs, ALP activity and alizarin red staining of calcium nodules were evaluated for SGPA's ability to promote bone formation. The results showed that GPA increased ALP activity, while SGPA was more significant (Fig. 3B–C). Furthermore, SGPA significantly enhanced the mineralization of OBs (Fig. 3D).

3.4. SGPA promotes bone formation and treat osteoporosis

To evaluate the anti-osteoporosis activity in vivo with SGPA, SGPA administration was used to treat OVX-induced osteoporosis mice. Micro-

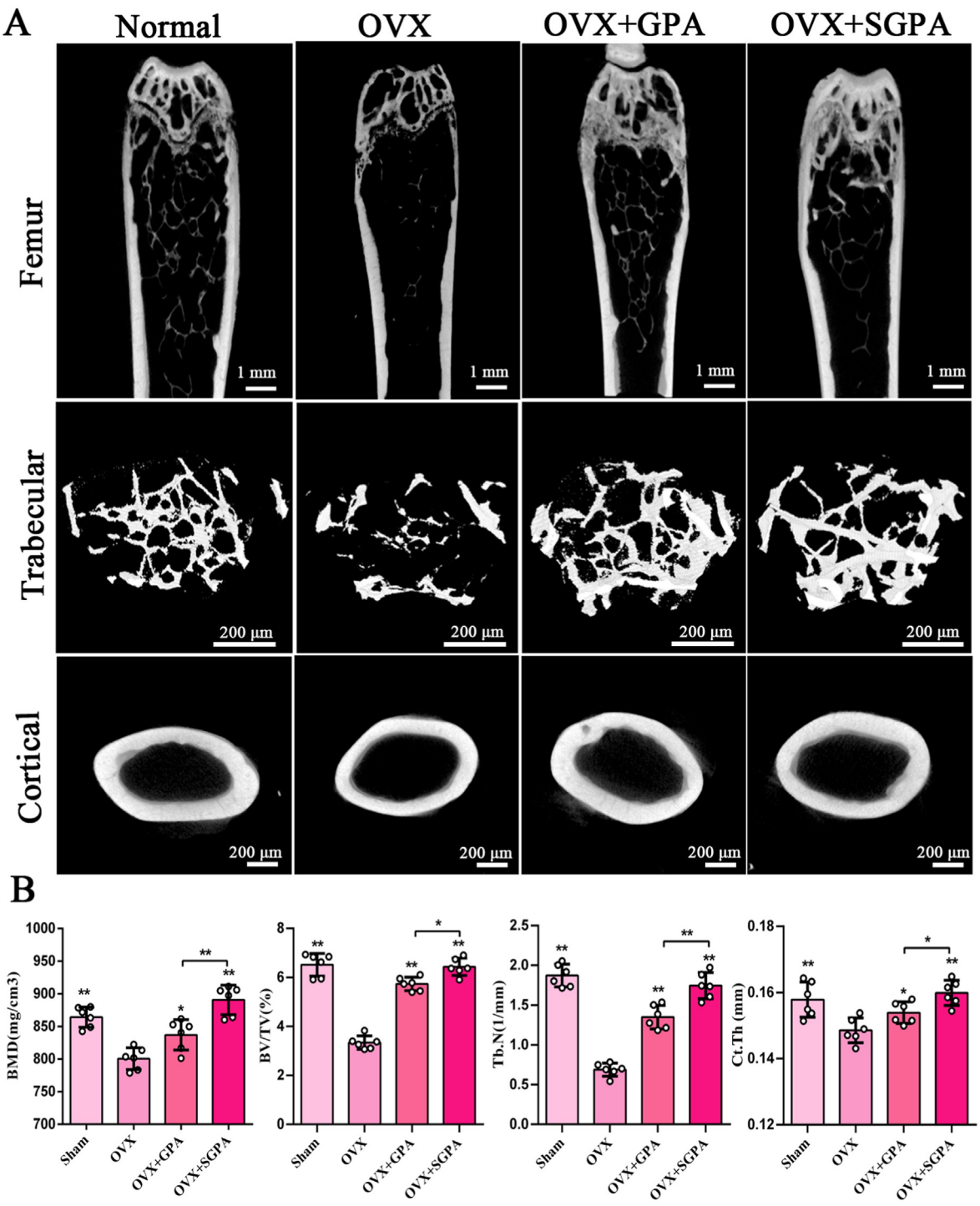

Figure 4. SGPA promotes bone formation and treat osteoporosis. (A) Femur, trabecular and cortical bone structures were performed by μCT and postprocessed by 3D computer reconstruction (n = 6). (B) The quantitative analysis of bone microstructure-related parameters including BMD, BV/TV, Tb.N and Ct. Th. Data are presented as the means ± S.D. n.s not significant, $^{*}P < 0.05$, $^{**}P < 0.01$.

CT was performed to evaluate whether the SGPA intervention in bone formation resulted in changes to bone mass. Indeed, SGPA treatment significantly increased the trabecular bone mass of the mice (Fig. 4A). Consistently, the quantitative analyses including BMD, BV/TV, Tb.N and Ct. Th all showed significantly increased bone mass and density in the femurs of the SGPA-treated mice (Fig. 4B). Furthermore, the double labelling of xylenol orange and calcein suggested that the mice after SGPA administration have a higher bone mineralization deposition rate than the GPA-treated mice (Fig. 5A–B). Similarly, SGPA significantly enhanced serum BALP and P1NP levels (Fig. 5C). Therefore, SGPA improves bone biological properties and bone formation of OVX-induced osteoporotic mice significantly.

3.5. *SGPA promotes bone formation by activating osteoblast FXR-RUNX2 signalling*

Our studies demonstrate that RUNX2 level is activated by FXR in osteoblast lineage cells [26]. To determine whether SGPA regulates

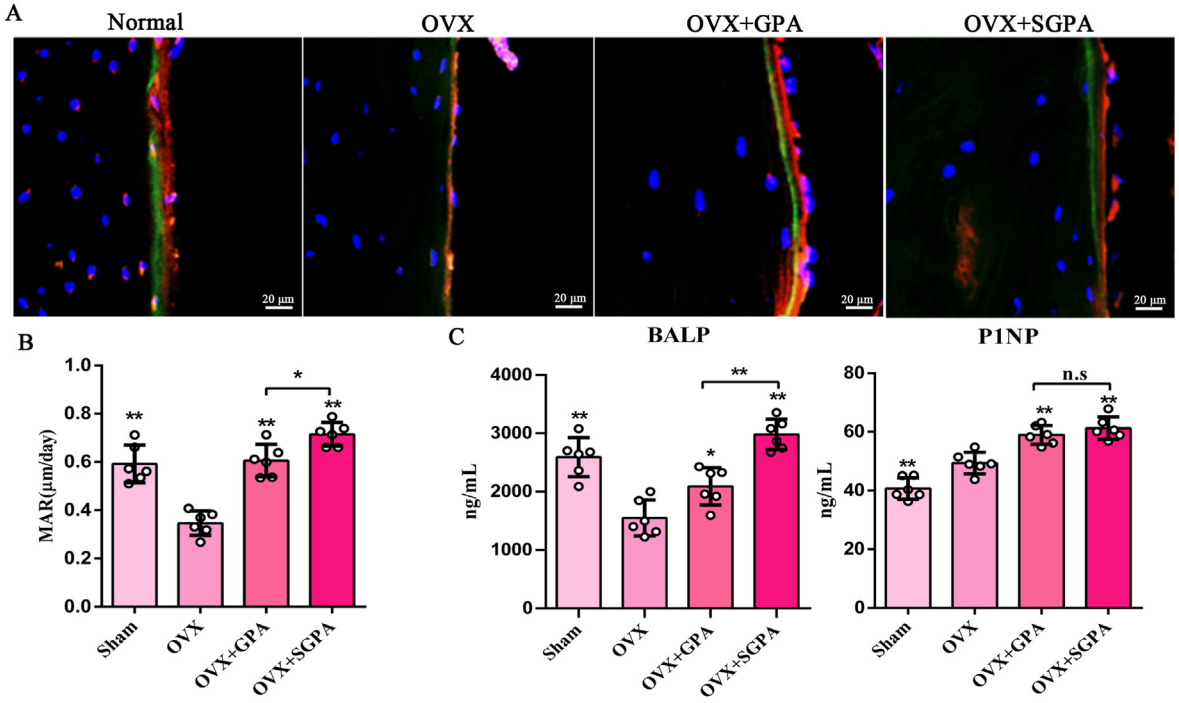

Figure 5. SGPA promotes bone formation in vivo. (A) A representative fluorescence image of femur (magnification, 400 ×) after xylenol orange (red) and calcein labelling (green) (n = 6). (B) Dynamic histomorphometric analyses of femur mineral apposition rate (MAR) (n = 6). (C)The levels of bone formation biomarkers (ALP, P1NP in serum) were measured using ELISA kit (n = 6). Data are presented as the means ± S.D., $^{*}P < 0.05$, $^{**}P < 0.01$.

FXR-RUNX2 signalling, we analysed the mRNA and protein expression of Bsep and Runx2 in femur. We found that the mRNA expression Bsep (a target gene for FXR) and Runx2 were significantly increased in GPA-treated mice, but were higher in the SGPA-treated mice than in the GPA-treated mice (Fig. 6A), and protein levels analysis was the same (Fig. 6B). Notably, compare with GPA, SGPA significantly upregulated RUNX2 levels in femur (Fig. 6C). Consistent with this, SGPA does activate the FXR-RUNX2 signalling in vitro (Fig. S2). These findings demonstrate that SGPA also activates FXR-RUNX2 signalling in OBs, with a more significant effect than GPA.

4. Discussions

Osteoporosis is a disease that requires long-term treatment. To achieve low-dose drugs accurate delivery to bone tissue and avoid adverse reactions in non-bone tissue, bone-targeted drugs that specifically act on bone tissue has become the focus. The osteoblast lineage is of great interest in cellular-targeted drug research owing to its implications in bone development and disease [27]. In 2015, Liang et al. successfully screened the nucleic acid aptamer CH6 targeting OBs using the systematic evolution of ligands by exponential enrichment (SELEX) technology, and combined with liposome nanoparticles, Plekho1 siRNA was delivered to OBs to promote bone formation [18]. In 2016, Sun et al. screened the specific osteoblast-targeting peptide SDSSD, and combined with polyurethane (PU) nano-micelles, anti-miR-214 was delivered to OBs [21]. However, the delivery of natural compounds to OBs using these targeting molecules is unknown.

GPA is a natural compound of iridoid glycosides, and its core structure is a better natural biological cross-linking agent, which can be cross-linked with protein, collagen, gelatin, etc. to make biomedical materials, such as artificial bones and wound dressing materials [28,29]. Structurally, GPA provides an active hydroxyl group for conjugation with the osteogenic targeting peptide SDSSD. In terms of efficacy, GPA was extracted from *Eucommia ulmoides*, a classical traditional Chinese herbal medicine, has been used to treat osteoporosis widely [30]. In this study, using Fmoc peptide synthesis and coupling method, GPA was directly coupled with SDSSD to form a new conjugate SGPA, which resulted in the accumulation of OBs in bone tissue and promoted osteogenic activity.

OBs are the main functional cells in bone formation and are responsible for the synthesis, secretion, and mineralization of bone matrix. In the process of osteoblast differentiation and maturation, specific markers such as ALP, osteocalcin, and PINP are gradually expressed [31,32]. At the same time, in this process, OBs are regulated by a series of transcription factors, such as Runt-related transcription factor 2 (Runx2), Osterix/SP7, transcription activator 4, Smad4, β-catenin [27,33,34], which act synergistically to regulate osteogenesis. In our study, SGPA enriched in OBs, activated FXR in osteoblasts and up-regulated Runx2 levels, and was accompanied by an increase in the content of ALP and P1NP. Notably, in vitro SGPA enhanced osteoblast activity and mineralization at lower doses than GPA. At the same dose, in vivo SGPA has a better effect on promoting bone formation in treating osteoporosis, compared with GPA.

5. Conclusion

In summary, we have successfully constructed SGPA, a new conjugate of GPA modified by osteoblast-targeting peptide SDSSD, confirming that SGPA enriched into osteoblasts and promoted bone formation at relatively low doses, provides a new idea for the targeted delivery and safe application of natural compound GPA in treating osteoporosis.

6. Ethical approval statement

All animal studies described herein were approved by the Institutional Animal Care and Use Committee of Beihang University (NO: BM20200046).

Author contributions

Meijing Liu and Xiaogang Wang conceived and designed the study; Meijing Liu, Danqi Zhu, Fujun Jin, and Shuang Li performed the experiments; Meijing Liu, Danqi Liu, and Xiangning Liu analysed the data;

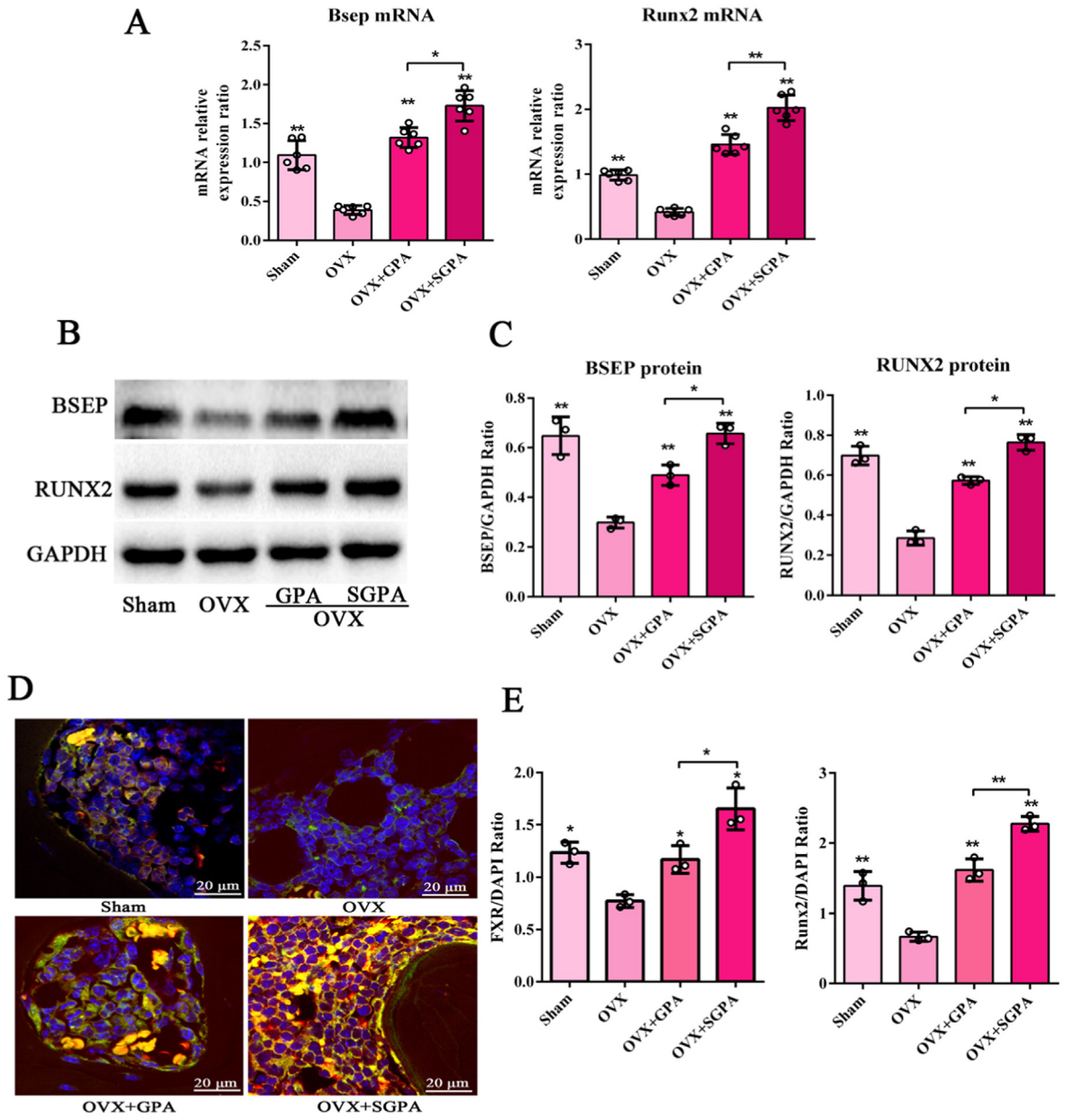

Figure 6. SGPA activating osteoblast FXR-RUNX2 signalling in vivo. (A) The mRNA expression of Bsep and Runx2 in bone tissues of OVX-induced osteoporosis mice were analysed by qRT-PCR (n = 6). (B–C) The representative western blotting analysis and relative quantification of BSEP and RUNX2 protein levels in bone tissues of OVX-induced osteoporosis mice (n = 3). (D) Immunostaining of FXR (green) and Runx2 (red) on femur tissue of OVX-induced osteoporosis (magnification, 630 ×). (E) The relative quantification of FXR and Runx2 levels in femur (n = 3). Data are presented as the means ± S.D. n.s not significant, $^{*}P < 0.05$, $^{**}P < 0.01$.

Meijing Liu, Fujun Jin and Xiaogang Wang wrote and revised the manuscript.

Conflict of interest

The authors declare that there are no conflicts of interest.

Acknowledgments

This work was supported by the National Natural Science Foundation of China (No. 82002362, 92049201), General Financial Grant from the China Postdoctoral Science Foundation (No. 2021M701421).

Appendix A. Supplementary data

Supplementary data to this article can be found online at https://doi.org/10.1016/j.jot.2022.07.007.

References

[1] Hernlund E, Svedbom A, Ivergard M, Compston J, Cooper C, Stenmark J, et al. Osteoporosis in the European union: medical management, epidemiology and economic burden. A report prepared in collaboration with the international osteoporosis foundation (IOF) and the European federation of pharmaceutical industry associations (efpia). Arch Osteoporos 2013;8:136.
[2] Curry S, Krist A, Owens D, Barry M, Caughey A, Davidson K, et al., US Preventive Services Task Force. Screening for osteoporosis to prevent fractures: US preventive services task force recommendation statement. JAMA 2018;319(24):2521–31.
[3] Zeng Q, Li N, Wang Q, Feng J, Sun D, Zhang Q, et al. The prevalence of osteoporosis in China, a nationwide, multicenter DXA survey. J Bone Miner Res 2019;34(10):1789–97.

[4] Compston JE, McClung ME, Leslie WD. Osteoporosis. Lancet 2019;393:364–76.
[5] Saag KG, Petersen J, Brandi ML, Karaplis AC, Lorentzon M, Thomas T, et al. Romosozumab or alendronate for fracture prevention in women with osteoporosis. N Engl J Med 2017;377(15):1417–27.
[6] Ha H, Ho J, Shin S, Kim H, Koo S, Kim IH, et al. Effects of Eucommiae Cortex on osteoblast-like cell proliferation and osteoclast inhibition. Arch Pharm Res (Seoul) 2003;26(11):929–36.
[7] Zhang R, Liu ZG, Li C, Hu SJ, Liu L, Wang JP, et al. Du-Zhong (Eucommia ulmoides Oliv.) cortex extract prevent OVX-induced osteoporosis in rats. Bone 2009;45(3): 553–9.
[8] Chen H, Huang X, Min J, Li W, Zhang R, Zhao W, et al. Geniposidic acid protected against ANIT-induced hepatotoxity and acute intrahepatic cholestasis, due to Fxr-mediated regulation of Bsep and Mrp2. J Ethnopharmacol 2016;179:197–207.
[9] An J, Hu F, Wang C, Zhang Z, Yang L, Wang Z. Pharmacokinetics and tissue distribution of five active ingredients of Eucommiae cortex in normal and ovariectomized mice by UHPLC MS/MS. Xenobiotica 2016;46(9):793–804.
[10] Cheng C, Du F, Yu K, Wang F, Li L, Olaleye OE, et al. Pharmacokinetics and disposition of circulating iridoids and organic acids in rats intravenously receiving ReDuNing injection. Drug Metab Dispos 2016;44(11):1853–8.
[11] Cho SW, An JH, Park H, Yang JY, Choi HJ, Kim SW, et al. Positive regulation of osteogenesis by bile acid through FXR. J Bone Miner Res 2013;28(10):2109–21.
[12] Forman BM, Goode E, Chen J, Oro AE, Bradley DJ, Perlmann T, et al. Identification of a nuclear receptor that is activated by farnesol metabolites. Cell 1995;81:687–93.
[13] Stapleton M, Sawamoto K, Alméciga-Díaz CJ, Mackenzie WG, Mason RW, Orii T, et al. Development of bone targeting drugs. Int J Mol Sci 2017;18(7):E1345. pii.
[14] Wang D, Miller SC, Kopecková P, Kopecek J. Bone-targeting macromolecular therapeutics. Adv Drug Deliv Dev 2005;57(7):1049–76.
[15] Wang H, Liu J, Tao S, Chai G, Wang JP, Hu F, et al. Tetracycline grafted PLGA nanoparticles as bone targeting drug delivery system. Int J Nanomed 2015;10(5): 678–85.
[16] Hengst VC, Kissel OT, Storm G. Bone targeting potential of BP targeted liposomes: preparation, characterization and hydroxyapatite binding in vitro. Int J Pharm 2007;331:224–7.
[17] Pontikoglou C, Deschaseaux F, Sensebé L, Papadaki HA. Bone marrow mesenchymal stem cells:Biological properties and their role in hematopoiesis and hematopoietic stem cell transplantation. Stem Cell Rev Rep 2011;7:569–89.
[18] Liang C, Guo B, Wu H, al e. Aptamer functionalized lipid nanop articles targe ting osteoblasts as a novel RNA interference based bone anabolic strategy. Nat Med 2015;21:288–94.
[19] Pillinger G, Loughran NV, Piddock RE, Shafat MS, Zaitseva L, Abdul-Aziz A, et al. Targeting PI3Kδ and PI3Kγ signalling disrupts human AML survival and bone marrow stromal cell mediated protection. Oncotarget 2016;7:39784–95.
[20] Sekiya I, Larson BL, Vuoristo JT, Cui JG, Prockop DJ. Adipogenic differentiation of human adult stem cells from bone marrow stroma (MSCs). J Bone Miner Res 2004; 19:256–64.
[21] Sun Y, Ye X, Cai M, Liu X, Xiao J, Zhang C, et al. Osteoblast-targeting-peptide modified nanoparticle for siRNA/microRNA delivery. ASC Nano 2016;10(6): 5759–68.
[22] Carbone EJ, Rajpura K, Allen BN, Cheng E, Ulery BD, Lo KW. Osteotropic nanoscale drug delivery systems based on small molecule bone-targeting moieties. Nanomedicine 2017;13(1):37–47.
[23] Sun Y, Cai M, Zhong J, Yang L, Xiao J, Jin F, et al. The long noncoding RNA lnc-ob1 facilitates bone formation by upregulating Osterix in osteoblasts. Nature Metabolism 2019;1:485–96.
[24] Bakker AD, Klein-Mulend J. Osteoblast isolation from murine calvaria and long bones. Methods Mol Biol 2012;816:19–29.
[25] Maridas DE, Rendina-Ruedy E, Le PT, Rosen CJ. Isolation, culture, and differentiation of bone marrow stromal cells and osteoclast progenitors from mice. JoVE 2018;131:56750.
[26] Liu M, Jin F, Zhang S, Li S, Zhu D, Cui Y, et al. Activation of farnesoid X receptor signaling by geniposidic acid promotes osteogenesis. Phytomedicine 2022; 102(2022):154258.
[27] Salhotra A, Shah HN, Levi B, Longaker MT. Mechanisms of bone development and repair. Nat Rev Mol Cell Biol 2020;21(11):696–711.
[28] Hu B, Xie M, Zhang C, Zeng X. Genipin-structured peptide-polysaccharide nanoparticles with significantly improved resistance to harsh gastrointestinal environments and their potential for oral delivery of polyphenols. J Agric Food Chem 2014;62(51):12443–52.
[29] Liu Y, Dai Q, Wang S, Deng Q, Wu W, Chen A. Preparation and in vitro antitumor effects of cytosine arabinoside-loaded genipin-poly-l-glutamic acid-modified bacterial magnetosomes. Int J Nanomed 2015;10:1387–97.
[30] Wu L, Ling Z, Feng X, Mao C, Xu Z. Herb medicines against osteoporosis: active compounds & relevant biological mechanisms. Curr Top Med Chem 2017;17(15): 1670–91.
[31] Vimalraj S. Alkaline phosphatase: structure, expression and its function in bone mineralization. Gene 2020;754:144855.
[32] Qin X, Jiang Q, Komori H, Sakane C, Fukuyama R, Matsuo Y, et al. Runt-related transcription factor-2 (Runx2) is required for bone matrix protein gene expression in committed osteoblasts in mice. J Bone Miner Res 2021;36(10):2081–95.
[33] Soltanoff CS, Yang S, Chen W, Li Y. Signaling networks that control the lineage commitment and differentiation of bone cells. Crit Rev Eukaryot Gene Expr 2009; 19(1):1–46.
[34] Komori T. Regulation of osteoblast differentiation by transcription factors. J Cell Biochem 2006;99(5):1233–9.